SORGHUM HIGH-THROUGHPUT PHENOTYPING PLATFORM FOR GREENHOUSES

A Thesis

by

JOSE ALEJANDRO BATZ ALVARADO

Submitted to the Office of Graduate and Professional Studies of
Texas A&M University
in partial fulfillment of the requirements for the degree of

MASTER OF SCIENCE

Chair of Committee,	J. Alex Thomasson
Committee Members,	John Mullet
	Sandun Fernando
Head of Department,	Stephen Searcy

December 2016

Major Subject: Biological and Agricultural Engineering

ABSTRACT

Plant phenotyping involves collecting information on the physical characteristics of plants. The information collected assists breeders and biologists to improve desired traits in crops. It is crucial to understand the behavior of crop plants in controlled settings so that genetic differences can be observed. In this period of increasing energy demand, renewable and carbon-neutral energy sources have become the subject of more research. One crop that is a possible biomass-energy source is energy sorghum, which does not compete as food source and is efficient at accumulating biomass. The stalk-thickness and height of energy sorghum are the main phenotypic parameters of interest, because 70-80 percent of the biomass is stored in the stalk. Measuring the stalk of energy sorghum can enable estimation of biomass yield. However, a phenotyping system dedicated to high-throughput data collection in energy sorghum in a greenhouse has yet to be developed. The research presented herein details the design, construction and testing of a semi-automated phenotyping system for energy sorghum plants in a greenhouse. Image collection, processing and analysis are evaluated as a potential method for measuring plant stalk thickness. The system proved capable of collecting digital images of 288 energy sorghum plants – a representative number for the greenhouse in the study – in 10.5 hours. Images were collected with 75% overlap and were stitched together manually with the GIMP software package to obtain a complete image of an individual plant. K-means segmentation was used to separate plant matter from background in the images, and a stalk-measurement algorithm was developed. Results of these image

analysis techniques provided an average of 16% error as compared to measurements obtained with a caliper. The results of this research suggest that this phenotyping method is viable, with high-throughput and mainly limited by image stitching.

ACKNOWLEDGEMENTS

I thank God for His grace through Jesus Christ that I have received abundant blessings, daily strength, and wisdom. It is because of His grace that amazing people have been present in my life, who devoted time and effort to assist me during the course of my studies. There were many, however, I would like to thank several of those people by name:

To Dr. Thomasson, for his consistent trust, guidance and support through the time of my research. It was because of the trust he had in me that I learned, giving me the opportunity to gain knowledge and skills. Dr. Thomasson, your continuous guidance and support, motivated me in the right direction and towards a successful project.

To Dr. Mullet and Dr. Fernando, my committee members, for being understanding and willing to assist when possible. Thank you for guidance and support.

To Brock Weers, research assistant scientist from the Department of Biochemistry and Biophysics at Texas A&M University, for growing all the plants used in this research. Thank you for devoting time to growing and maintaining the plants in the greenhouse. Without your expertise in this area, conducting my research would have been difficult.

To Mario Mendez, fellow research assistant and friend, for his outstanding support through this research. Thank you for your help, answering all those questions, from simple loops in a program to highly technical questions. Your wisdom and vast

knowledge in machinery and programming helped me through the challenges in my project.

To my parents, dad (papá) and mom (mamá), who have loved me unconditionally and provided everything on their behalf to support me during my time at Texas A&M University. Thank you for your constant prayers, asking for God's grace and care. Thank you for working endlessly and sacrificing many things so that you could provide for me.

To my sister Rosa, who was always there when I needed someone and for her unselfish support. Thank you for supporting me while in school, for your constant prayers, and for being a role model.

To my sister Gladys, who supported me and always believed in me. Thank you for your constant words of encouragement and showing me that giving up is not an option.

To Shane Cannon, religious mentor and friend, for being there for me and for providing a helping hand. Thank you for your constant prayers, and mending me to trust in the Lord.

To Cheikh Beye, Walter Oosthuizen, and Bryce Wingate, my closest friends, for the great experience at Texas A&M University. Thank you for your constant support, for showing me through example that I could achieve my goals. Also, thanks for all the funny and memorable moments, which are cherished for life.

To all the faculty and staff in the Department of Biological and Agricultural Engineering, for their assistance through the time of my research.

CONTRIBUTORS AND FUNDING SOURCES

Contributors

Part 1, faculty committee recognition

This work was supervised by a thesis committee consisting of Professor Alex Thomasson of the Department of Biological and Agricultural Engineering and Professors John Mullet of the Department of Biochemistry and Biophysics and Sandun Fernando of the Department of Biological and Agricultural Engineering.

Part 2, student/collaborator contributions

The energy sorghum plants used through the course of this research were provided by Dr. Mullet and maintained by Brock Weers, both from the Department of Biophysics and Biochemistry at Texas A&M University.

All other work conducted for the thesis was completed by the student independently.

Funding Sources

This work was made possible in part by the Texas A&M AgriLife Bioenergy Program. Founding was also received from the ARPA-e TERRA program.

Its contents are solely the responsibility of the authors and do not necessarily represent the official views of the Texas A&M AgriLife Bioenergy Program or ARPA-e TERRA program.

TABLE OF CONTENTS

Page

LIST OF FIGURES

Page

LIST OF TABLES

Page

1. INTRODUCTION AND PROBLEM DEFINITION

1.1 Background

1.1.1 Plant Phenotyping and Importance

Plant phenotyping refers to the process of measuring and collecting information of the morphological parameters, behavior, and physiological attributes of plants. Both plant breeders and geneticists are interested in phenotypic data, as it helps to determine superior strains of crops and to understand changes in crop genes (Hartmann et al., 2011; Kipp et al., 2014; Rooney et al., 2007; Passioura, 2012; Walter et al., 2012). There have been recent advances in systems to collect phenotypic data on crop plants. One simple system has used a camera attached to a balloon to capture overhead images of crops (Lamb et al., 2014), and a more complex system has used a vehicle and various sensors to travel through crops and collect data (White et al., 2012; Andrade-Sanchez et al., 2014). The field of phenotyping is advancing rapidly, and particular crops often have multiple phenotyping requirements.

1.1.2 Research on Bioenergy Crops and Energy Sorghum

The increasing demand for renewable energy has generated interest in improving biofuel crops like energy sorghum. Of the total amount of energy consumed in 2013, 75.9% of the fuel was obtained from coal, petroleum and natural gas (IEA, 2015), and the increase in world population has created a constant increase in demand of energy from these fuels. Sources suggest that greenhouse gas (GHG) emissions, which are mainly generated from energy production, are a significant factor influencing climate change

(Gheorghe, 2015; Reuss, 2015; Watts, 2013). Renewable energy sources could provide a more secure long-term avenue for energy production as well as reduce GHG emissions (Koçar & Civas, 2013).

Crops such as corn and sorghum, which are already used for food and cattle feed, can serve as biofuel sources. Sorghum has advantages over corn as a biofuel, including a lower level of competition than corn for food-production land. Energy sorghum is a drought-tolerant crop with a fast growth rate and high biomass content and fast accumulation (Hao et al., 2014, Mullet et al., 2014). Developing improved energy sorghum plants is important to the future of bioenergy, and phenotyping is a critical need in this regard. Several morphological features are of importance when phenotyping energy sorghum, including stalk thickness and plant height, which are highly correlated to biomass accumulation of plants and shoot dry weight (Olson et al., 2012, Tazoe et al., 2016; Rooney et al., 2007). Between 70 and 85 percent of the total shoot biomass of energy sorghum is stored in the stalk of the plant (Rooney, 2016, personal communication; Olson et al., 2012). Plant height can be readily measured with an ultrasonic sensor or other sensing system, but a method has not yet been defined to measure stalk thickness rapidly and repeatedly.

1.1.3 Research in Plant Phenotyping

Sensor-based plant phenotyping in the broadest sense has been transitioning from large-scale aerial and satellite imaging of fields to high-resolution imaging of individual plants (Lamb et al., 2014; Mulla, 2013; Busemeyer et al., 2013; Green et al., 2012; Hund et al.,

2009, Tuberosa 2012). Digital imaging is now recognized as a non-invasive method to collect phenotypic data of individual plants (Busemeyer et al., 2013; Diago et al., 2012; Green et al., 2012). In addition to imaging, other sensors have been used for phenotyping in agriculture (Pajares et al., 2013). The GreenSeeker is a diffuse-reflectance sensor used to measure normalized difference vegetation index (NDVI) (Duda et al., 2016). Time-of-flight cameras are used for 3D image reconstruction and so are able to collect morphological information about plants. Multiple sensors can be mounted on platforms and used in the field for phenotyping (Busemeyer et al., 2013; Andrade Sanchez et al., 2013). The system presented by Busemeyer et al. (2013) uses a wide range of sensors including 3D time-of-flight cameras, hyperspectral imaging, a laser curtain, and ultrasonic sensors to measure plant height. This system enabled data collection of up to 2000 plots per day. All of these phenotyping systems have the objective of increasing the rate at which phenotypic data is collected without major disturbance to the plants.

1.1.4 Image Analysis and High-Throughput Phenotyping

Digital imaging with image analysis shows promise as an effective method to collect quantitative data of plants. Klukas et al. (2016) presented a study in which 33 maize plants were tracked, and 78 images of each plant were collected daily for a period of 64 days. From this experiment, 33,766 phenotypic measurements were obtained, including height, volume estimation, and leaf count. Visible, fluorescence and near-infrared (NIR) cameras were used to collect the images. The results of this study showed the possibility of using imaging systems to capture a large amount of data and analyze it in a timely

manner (Klukas et al., 2016). Gao et al. (2012) used image analysis in measuring leaf area from rose plants by determining the length and width of the plants. They found strong correlation between image-analysis results and manual methods ($R^2 = 0.917$). Golzarian et al. (2011) studied 320 plants for a period of six weeks in which the shoot dry weight of the plants was estimated with image analysis. The results showed that it was possible to differentiate between plants under salt stress with image-based estimates of shoot dry weight.

Capturing images of large plants at close range, such as in greenhouses or between field rows, is difficult due to the limitations of camera lenses at short distances from the plants. Heijden et al. (2012) designed a vertical system to solve the problem by suspending multiple cameras to simultaneously collect several images of pepper plants, which can extend to about 3 meters. This method, although a good solution, could become expensive if multiple cameras are used.

Phenotyping systems that employ digital imaging have used several image-analysis approaches to reveal phenotypic information (Busemeyer et al., 2013; Fraas & Lüthen, 2015; Hartmann et al, 2011). For example, Diago et al. (2012) utilized a clustering algorithm based on the Mahalanobis distance to identify grapes on grapevines. Singh et al. (2016) introduced different methods of machine learning for identification, classification, quantification, and prediction of plant stresses. Other methods of image analysis include Otsu's thresholding method and others like it to segment objects of interest (Granier et al., 2006; Hartmann et al., 2011; Olugbara et al., 2015). Numerous image analysis techniques for phenotyping systems have been developed and shared

through the Plant Image Analysis website [http://www.plant-image-analysis.org/]. Online systems and software-adaptable plug-ins such as PhenoPhyte and ImageJ, respectively, have been developed to assist with image analysis (Granier et al., 2006; Green et al., 2012).

In some cases, advanced camera systems are required to make certain phenotypic measurements such as advanced spectral reflectance, including NIR, and thermal imaging (Lamb et al., 2014; Lofton et al., 2012). The NIR band is often of particular interest since live plant material is highly reflective in this band (Dworak et al., 2013). NDVI is calculated from the red and NIR bands and gives useful information about the health and state of the plant (Barascu et al., 2016; Neiff et al., 2015; Dworak et al., 2013). Additionally, because there is higher reflectance in the NIR band for biological plant material than background objects, the complexity of image segmentation is mitigated with NIR. Color-infrared (CIR) imaging can be obtained with a CIR camera, and thermal imaging can potentially provide information of the water stress level of plants (Romano et al., 2011).

During breeding trials, in which numerous genetic lines of a plant type are compared, several rows of multiple plants are grown to minimize error in the data. As a result, a very high number of plants require evaluation (Singh et al., 2016), requiring a large number of manual measurements and a large amount of time. A needed advancement is to incorporate sensors onto mobile platforms for high-throughput phenotyping. Advantages of mechanized and automated phenotyping systems include (1) reducing the time it takes to repetitively collect similar data on multiple plants, rows, and plots; (2)

enabling measurements to be made in a short time window so as to minimize temporal variation; (3) potentially making more objective and accurate measurements; and (4) even making measurements that heretofore were unavailable.

The current state of the art includes systems that are relatively expensive and high-maintenance (Van Der Heijden, 2012). There isn't a current semi-automatic system capable of being used in multiple greenhouses dedicated to energy sorghum plants. If high-throughput phenotyping systems were available at a reasonable cost, breeders and geneticists could collect data much more efficiently and with more repetitions (Großkinsky et al., 2015; Mulla, 2013; Rooney et al., 2007), enabling them to consider many more genetic lines for faster crop improvement.

1.2 Objective

The objective of this project was to design, construct, and test a phenotyping system capable of collecting and analyzing multispectral images of complete energy sorghum plants in a greenhouse. Specific requirements of the system include a mobile sensing platform, capable of collecting images of all energy sorghum plants in a typical research greenhouse in 16 hours. The design number of plants was 288, and the design maximum plant height was 3.0 meters. The objective included image-analysis methods to measure stalk-thickness of energy sorghum. General design constraints included that the system be affordable, flexible, and low-maintenance.

2. METHODS AND MATERIALS*

2.1 Phenotyping System

2.1.1 Phenotyping System Requirements

The phenotyping system design consisted of a structure capable of carrying CIR, thermal and red, green and blue (RGB) band cameras. In order to make the system semi-automated, a motorized mechanism translated the cameras from side to side and up and down. A control station was implemented which consists of a touch screen with a user-friendly graphical user interface (GUI) and micro-computers to control the motors. In order to process and obtain phenotypic data from the images collected, a method for image mosaicking and image analysis was considered as part of the design. In summary, the following components and capabilities were required:

- A mobile phenotyping system
- A phenotyping system structure with low center of gravity for maneuverability
- An automatic articulation system for the cameras
- A user-friendly GUI control unit to control camera and sensor articulation
- Full plant image collection, for plants up to 3.0 meters tall
- Image mosaicking techniques
- Plant segmentation algorithm
- Stalk thickness measuring algorithm

*Part of this section is reprinted with permission from "Imaging for high-throughput phenotyping in energy sorghum" by Batz, J; Mendez-Dorado,M & Thomasson, J.A, 2016. Journal of Imaging, 2(4).

2.1.2 Mechanical Components

The design of the automated phenotyping platform was based on three structures (Figure 1): the bottom section, referred to as the support structure of the platform; the middle section, which consisted of a lift mechanism to increase the vertical reach of the upper section; and the upper section, a rectangular frame to hold the sensor system structure. All the structures were designed and modeled in SolidWorks 2013 software.

Two main factors were considered in determining the size of the platform: the configuration of the greenhouse and the size of energy sorghum plants. After surveying two greenhouses located at the Greenhouse Annex at Texas A&M University and developing a template of a possible greenhouse setup (Figure 2), the platform dimensions were determined.

The design size of the platform facilitated its movement in the greenhouse and prevented interference with the greenhouse structure. Due to the biomass storage quality of energy sorghum, it tends to grow tall. After taking manual measurements of sorghum height in the greenhouse, the average maximum height of mature sorghum was determined to range between 300 and 350 cm, with an average width span of 100 cm. The overall dimensions of the platform were 145 cm long, not including the push handle, 295 cm tall at the lowest position adjustment and 335 cm at the highest position adjustment, and 47 cm wide. At the highest position configuration, plants with a height up to 300 cm could be imaged.

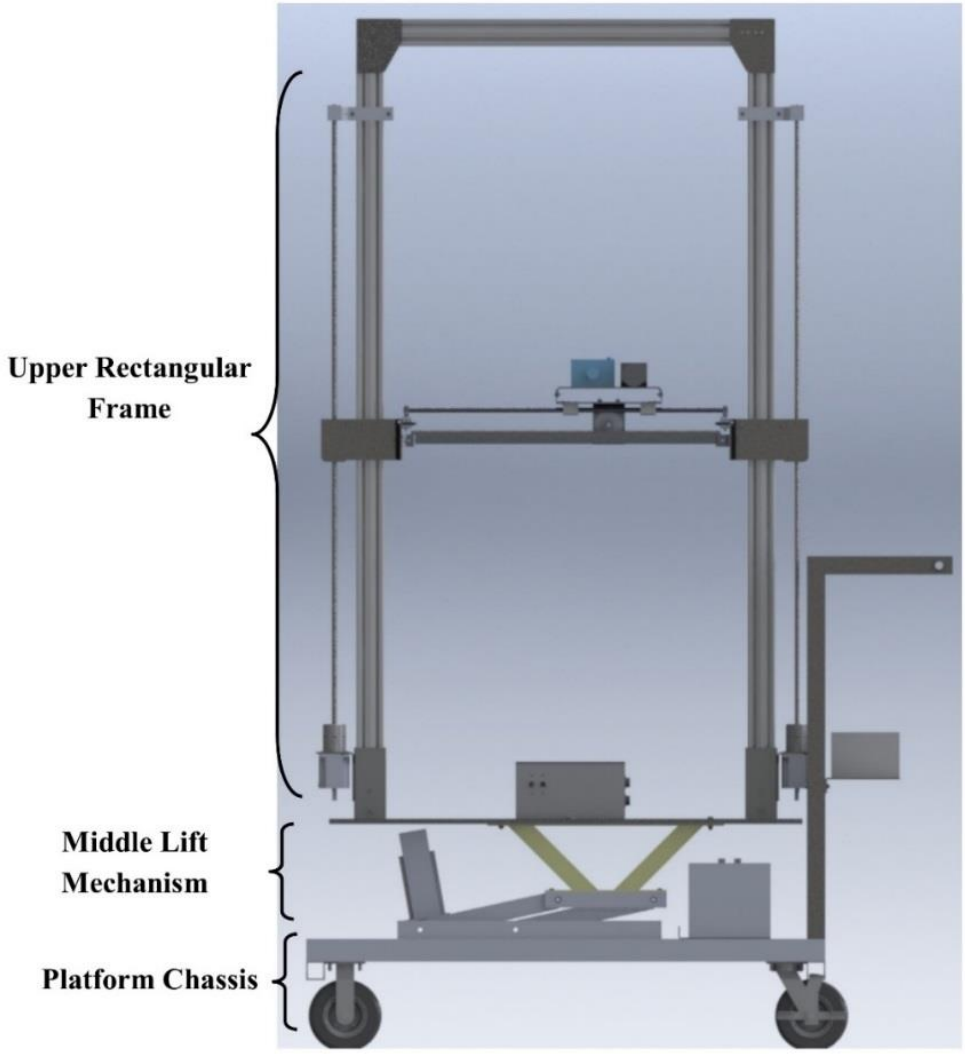

Figure 1. Phenotyping system design rendering, displaying the three sections of the design: Platform Chassis, Middle Lift Mechanism and Upper Rectangular Frame.

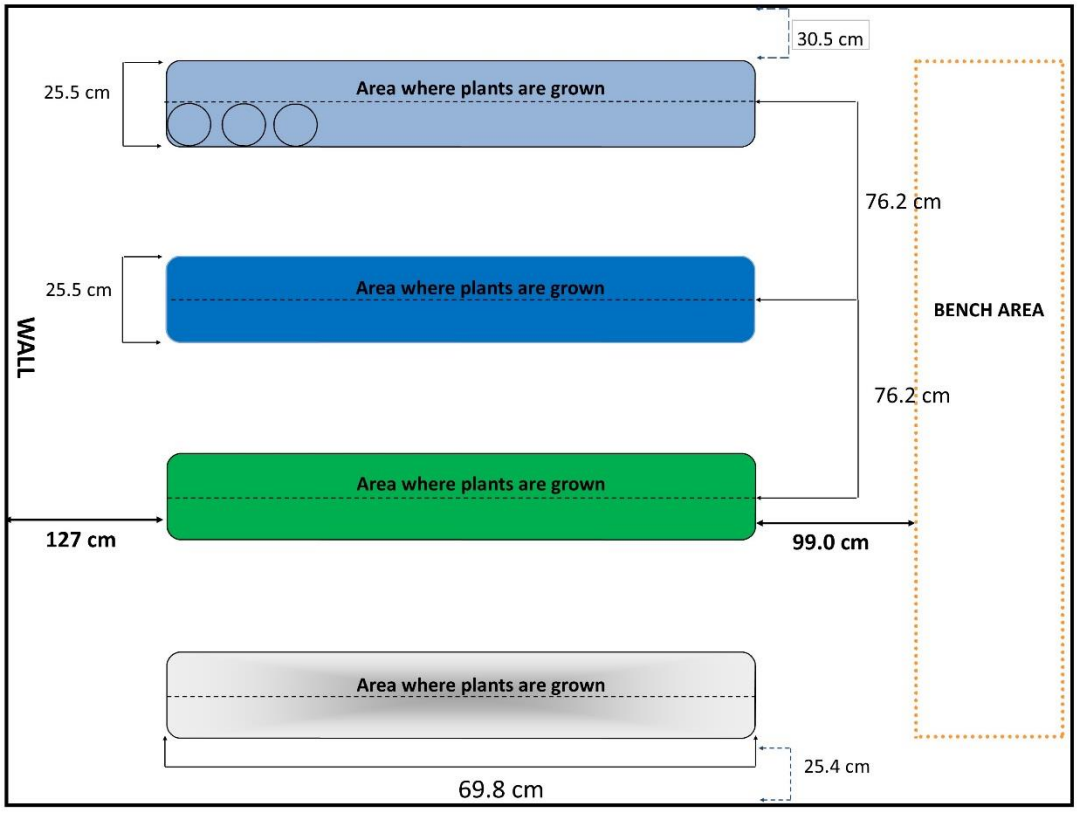

Figure 2. Top view of possible greenhouse layout where energy sorghum plants are to be grown.

2.1.2.1 Bottom Support Structure

The bottom support section, or platform chassis, was built from 6.35 cm mild steel square tubing with a thickness of 0.47 cm. The layout consisted of adjacent pairs of tubes, each pair placed 20.3 cm apart. Thus a 47.7 cm wide by 145 cm long frame was built and mounted on four wheels, two of which were swivel wheels to ease the handling of the platform. By using 20.3 cm diameter wheels, the platform chassis was suspended 26.0 cm above the ground, giving sufficient clearance to move through the greenhouse.

The steel tubing of the platform chassis gave the structure (Figure 3) a heavy bottom section and a low center of gravity, an important aspect of the design since the upper section included moving weight that could potentially cause the structure to tip over. An inverted L-shaped handle was added on the end with the swivel wheels. The handle provided a way to manually move and turn the platform, and it provided additional space to mount the control box unit.

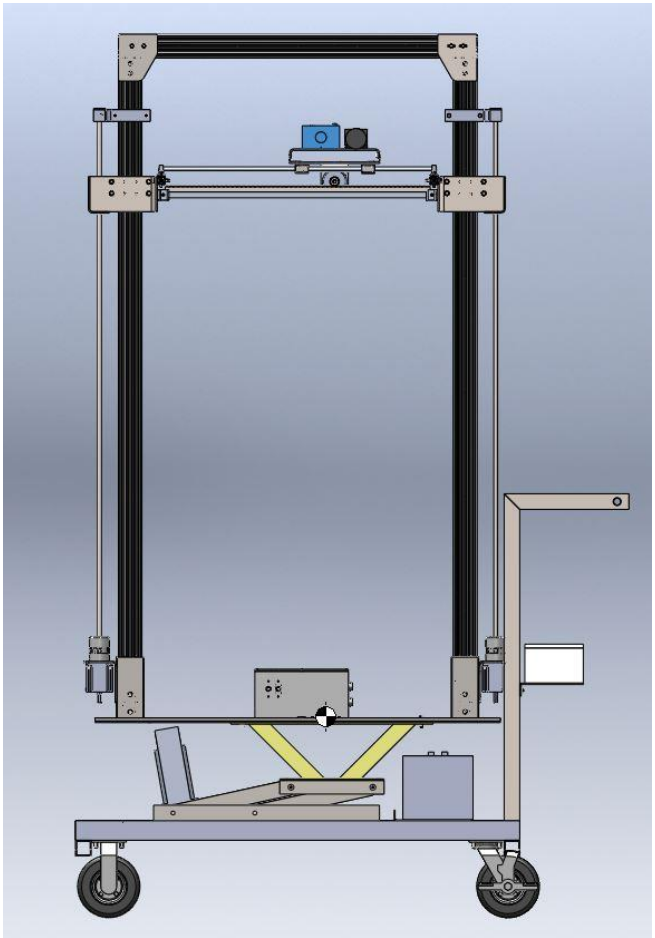

Figure 3. Phenotyping system design rendering, showing the estimated center of gravity in SolidWorks 2013.

2.1.2.2 Middle Lift Mechanism Structure

The lift mechanism consisted of a commercial-off-the-shelf (COTS) motorcycle lift (Pittsburgh Automotive – Harbor Freight Tools, [Camarillo, California, USA]) that was modified to fit the design. It was 40.6 cm wide and 68.6 cm long, with a maximum vertical extension of 40.6 cm and a load capacity of 450 kg. The lifting motion is actuated by a hydraulic cylinder, which is manually operated with a handle. The lift was placed on top of the chassis frame, so that the center of the lift was 45.8 cm from the edge where the handle was attached, and centered with respect to the two edges of the frame width (Figure 4). The lever that releases pressure from the hydraulic cylinder was extended, preventing the user from being under any part of the platform when it is lowered and therefore increasing operational safety and convenience. In the space between the lift and the platform handle, a plate (40.6 cm wide by 38.1 cm long by 0.476 cm thick) was added to provide a location for the batteries.

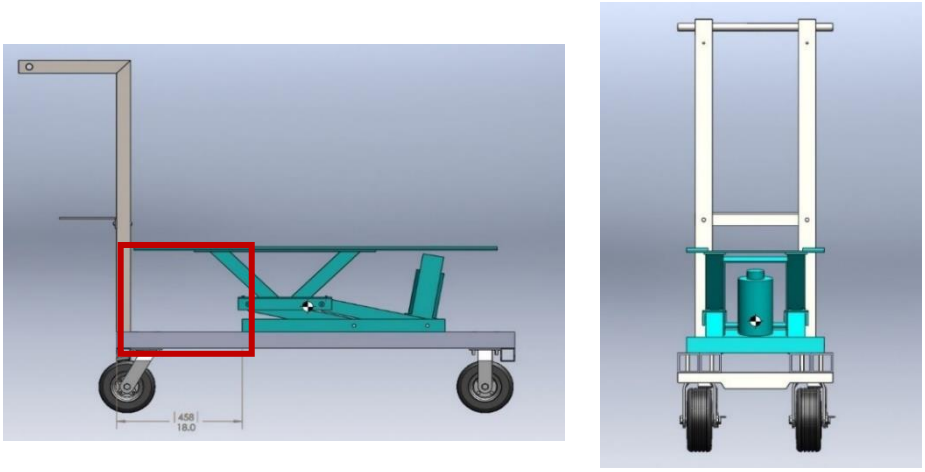

Figure 4. Design rendering, showing the Bottom Support Structure and the Middle Lift Mechanism. The red box indicates the location where the batteries was designed to fit.

A steel plate measuring 40.6 cm wide by 132 cm long by 0.635 cm thick was placed on top of the lift. In order to prevent interference between the plate and the hydraulic cylinder, a V-shaped structure was built (Figure 5). The V structure provided an offset of 26.0 cm, enough for the plate to clear the cylinder. The bottom of the V structure was attached to the lift and the top to the plate. To prevent bowing, the plate was reinforced along each long side with a strip of steel plate (7.62 cm wide by 132 cm long by 0.953 cm thick).

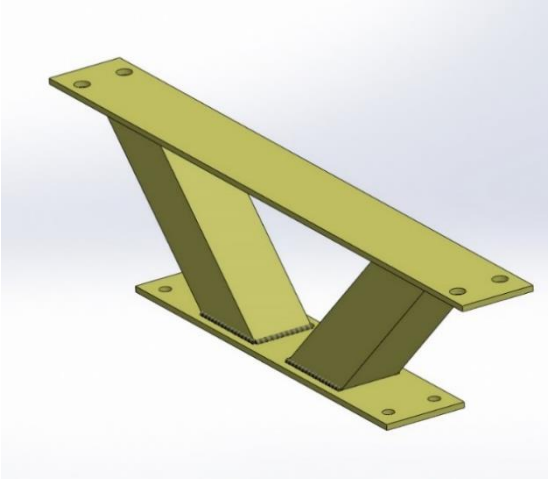

Figure 5. Design rendering of V-shaped structure added to design to prevent interference between the upper section structure of the phenotyping system and the hydraulic cylinder of the lift.

2.1.2.3 Upper Rectangular Frame

The imaging sensor system was placed within an upper rectangular frame. This structure (Frame_A; Figure 6), was built of 7.62 cm by 5.08 cm t-slotted aluminum extrusion bars. The vertical members measured 224 cm in length, while the horizontal member was 117 cm long. The vertical members were secured to the rest of the assembly with

custom “shoes”, and the horizontal member was secured to the vertical members with two steel plates on each corner.

Figure 6. Frame_A rendering, frame constructed of t-slotted aluminum extrusion bars, showing custom shoes for attachment to the rest of the phenotyping system. Additionally, the location of the motor placement along the vertical members of the frame is shown.

A stepper motor was attached to a threaded rod along the side of each vertical member with a lovejoy coupling. The threaded rod measured 165 cm long and 1.27 cm in diameter, and was secured at the top of the frame with a flanged bearing, allowing free rotation. Another structure (Frame_B) was designed to keep the two stepper motors moving vertically in unison with stable motion and negligible misalignment (Figure 7).

It was composed of a sled like sleeve-bearing, fitting between the channels of the vertical members of Frame_A; a wide nut for movement along the threaded rod; and support pieces to connect to the horizontal structure (Figure 7). One Frame_B was used on each vertical member. The horizontal structure consisted of a transverse 2.54 cm square tubing to bridge each Frame_B, and two horizontal rods, shown in Figure 8. A steel rack was mounted on the square tubing as part of the rack and pinion mechanism to move the imaging system from side to side.

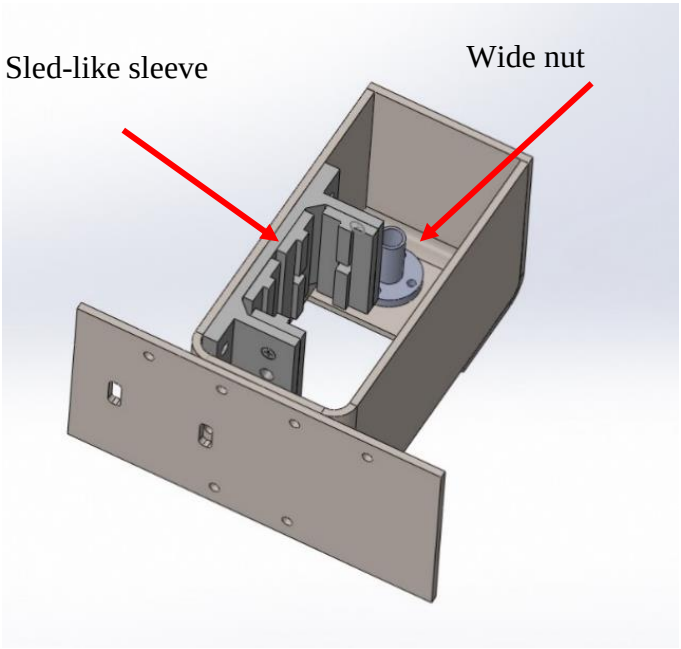

Figure 7. Frame_B rendering, structure added to each vertical member in Frame_A. The sled-like sleeve fit into the channels of the aluminum extrusion bars. The wide nut along with the threaded rod provided vertical motion.

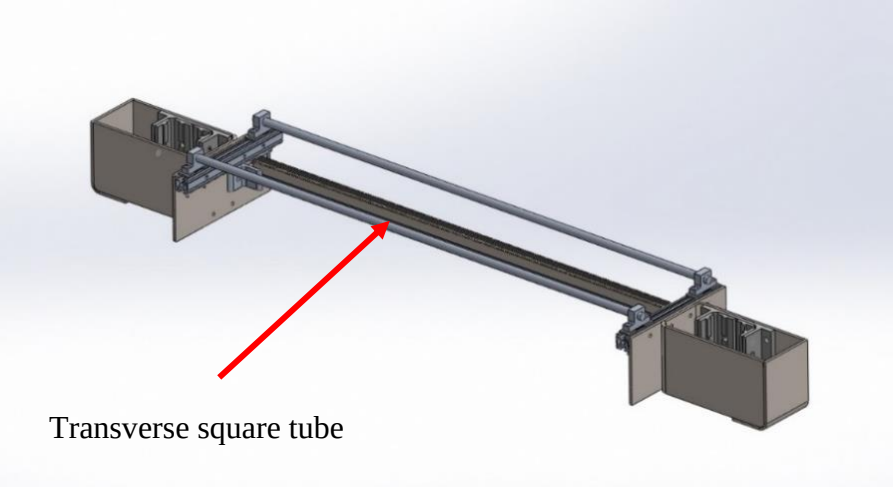

Figure 8. Design rendering showing the horizontal structure that connected both Frame B structures.

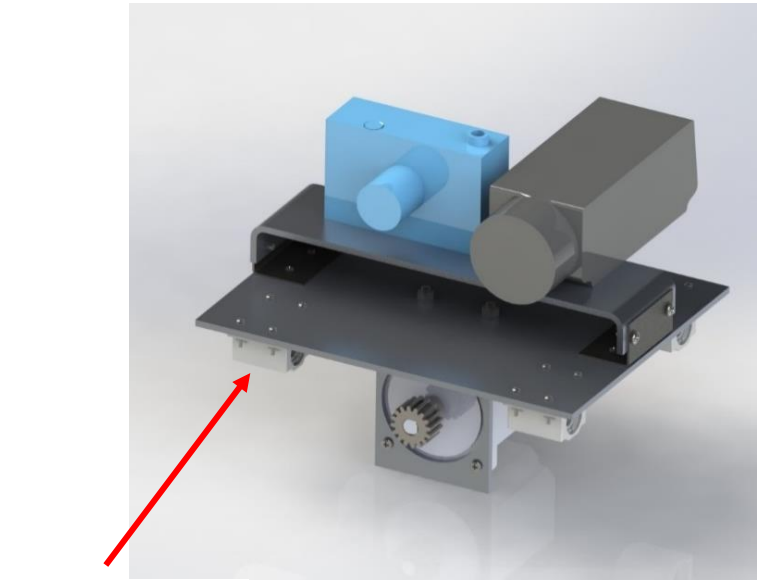

Figure 9. Frame_C structure rendering, it was designed to provide support to the imaging system. Four linear bearings supported the weight of the structure.

Within the upper frame, another structure (Frame_C) was designed to support the imaging sensor system (Figure 9). A 12.7 cm wide by 30.5 cm long by 0.476 cm thick steel plate was used to support the cameras and was attached to a lower plate that holds four linear bearings that slide over two rods horizontally. The weight of the cameras and any other components was therefore applied to the rods, reducing the possibility of damage to the gear head and rack due to grinding (Figure 10). The rods rested on the four bearings located on Frame_B. The pinion, part of the rack and pinion mechanism, was attached to a stepper motor.

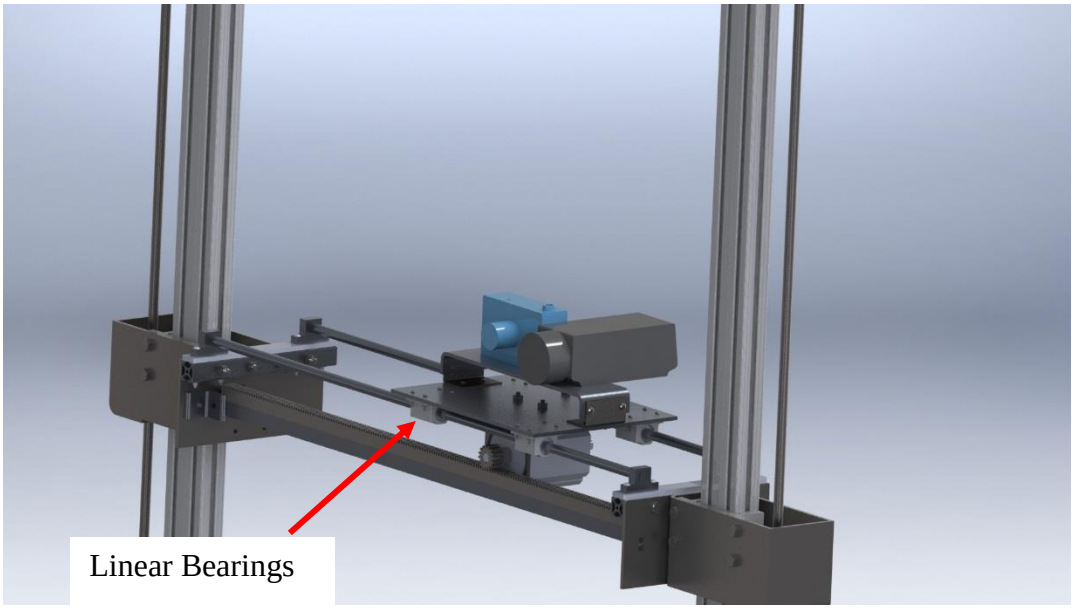

Figure 10. Rendering of Frame_C within Frame_A, showing the interaction between the linear bearings and the support rods.

2.1.3 Electronic Components

2.1.3.1 Imaging System

The sensor station was designed to house two cameras at the same time. However, for testing purposes, only one was used. The camera used in the current sorghum phenotyping work is a CIR camera (Table 1).

Table 1. Color infrared (CIR) camera specification: Agricultural Digital Camera.

Manufacturer:	Tetracam Inc. [Chatsworth, California, USA]
Max resolution:	2048 x 1536 pixels
Sensor:	3.2 Megapixel CMOS –filter blocking blue light and allowing NIR
Image Storage:	Compact Flash
Image Format storage:	Tetracam RAW or DCM
Power Requirement:	12 VDC, 500 mA

2.1.3.2 Motors and Controllers

Motors, controllers, and a control station were used to automate system operation. The phenotyping platform translated the imaging system from side to side and up and down with stepper motors (HT34-50 NEMA 34, Applied Motion Products, [Watsonville, California, USA]), selected because of their precise controllability and simplicity. Two assumptions were made to determine the torque necessary to move the structure vertically, so that adequate motors for this application could be determined. (1) The total force created by the weight of the structure will be distributed at the two points of

contact, between each wide nut and threaded rod. (2) The maximum force applied on either side is based on the total mass of Frames B and C, which was about 11.3 kg, resulting in a force of 110.5 N. When Frame_C moves to either side, the applied force changes on both sides. It is assumed that in the extreme case, the entire structure is on one side. The starting torque required to counter 110.5 N upward by one motor was calculated to be 1.40 N•m (Equations 1-3, from Norton, 2015). Each motor selected is able to produce a bipolar torque of 6.00 N•m, giving a factor of safety (f.s) of 4.28. Such a large f.s. allows the design to carry additional weight from the sensors without having to replace the motors or the structure.

$$Tu = Tsu + Tc \quad (1)$$

$$Tsu = \left(\frac{P*dp}{2}\right) * \left(\frac{\pi*u*dp+L*Cos(angle)}{\pi*u*Cos(angle)-u*L}\right) \quad (2)$$

$$Tc = uc * P * dc * 0.5 \quad (3)$$

Where:

Tu = Total torque to lift load
Tsu = Total torque required to lift load
Tc = Total friction torque between screw-nut interface
P = total load
dp = pitch diameter
u = dynamic friction factor
L = Screw traveled distance
angle = screw angle
uc = static friction factor

The motors were rated as high–torque, with the maximum bipolar torque at 2 RPM, and a step angle up to 1.8 degrees. These motors are capable of operating in a range from 200 to 20000 steps per revolution, the higher numbers with micro-stepping. Precision is

inversely related to the speed of the motor, but since this application did not require extreme precision, the motors were set to 400 steps per revolution. At this rate, and with the assistance of the fast threading rods, the motors could translate the imaging system at 6 cm per second. The maximum torque for these motors required 6.5 amperes (A) from a 24-volts (V) power supply. When the power requirements are not met, the stepper motor controller trips and sets an alarm, so for safe operation each motor was assumed to require a minimum of 7 A. The motors were controlled by stepper motor drivers (STR8 – DC Advanced Microstep Drive, Applied Motion Products). These motor controllers feature direction and speed control, and were placed along with the power distribution system in an enclosed box measuring 30.5 x 30.5 x 12.3 cm, large enough to allow for adequate ventilation of the controllers.

2.1.4 Control Station Unit

The platform motors were controlled by the control station with a user-friendly GUI. The control station consisted of a plastic enclosure measuring 20 cm wide by 20 cm long by 13 cm high. Inside the control station box were microcontrollers and electronic components.

Instead of using a keyboard and mouse, a touchscreen was surface mounted to the top of the control station box (Figure 11), providing easy access to input commands in the GUI. A Raspberry Pi 2 (RPi) microcontroller (model B, Raspberry Pi Foundation, [Caldecote, Cambridgeshire, United Kingdom]) was used to generate the GUI. Although the RPi is easy to program and useful for basic control functions, it has its limitations. The RPi is unable to execute in nearly real-time. There is a delay each time the RPi

outputs a logical value (i.e. 0 or 1). The stepper motor controllers must receive a logical value-specific sequence and time to operate correctly. In order to compensate for the delay, an Arduino Uno Board (Arduino.cc & Adafruit, [New York City, New York, USA]) was added to the imbedded control system. The Arduino board and RPi are able to communicate via USB serial protocol. An array composed of four bits (or a nib) is sent to the Arduino from the RPi, each for a specific task. The Arduino board is dedicated to outputting logical values to the stepper controllers, which then actuate the motors. Another limitation of the RPi is the ability to keep track of time accurately. In response, a ChronoDot RTC system (Adafruit, [New York City, New York, USA]) was used to provide time stamps on data collected. The control station design was made detachable such that it would be connected only each time the platform was used, reducing the chance of water damage to the electronic components. Easy connectors were added to the box to reduce setup time when the phenotyping system was used.

In the GUI, a mode can be selected in which the user can input the height of a single plant sample, and the RPi will then control the location of the imaging system and the number of image-collection points that will represent the entire plant. A jog mode (manual mode) can also be selected in which the user is able to move the imaging system manually. A limit was written into the system software, such that after a certain distance is traveled, the system will not continue moving. The distance traveled is calculated by the RPi, keeping track of the number of steps each motor moves. This safety system prompts the user when the limit has been reached and stops the motors automatically to prevent collision with the upper frame.

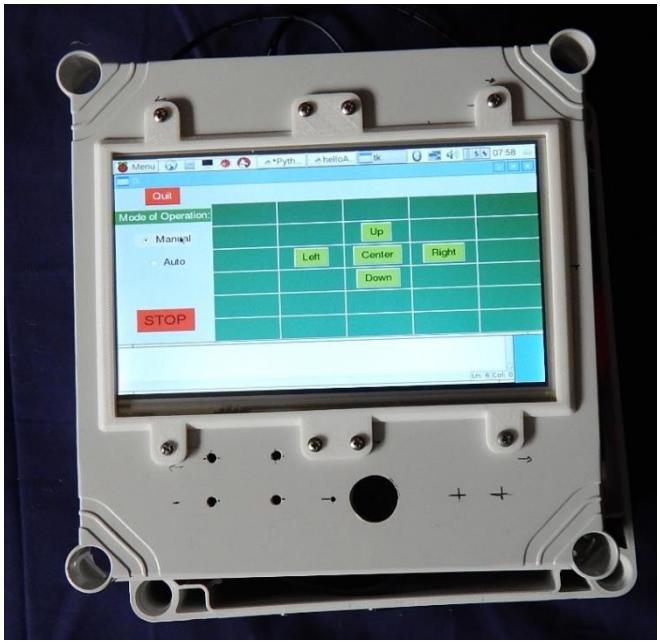

Figure 11. Control station box design, showing the touchscreen and designed graphic user interface (GUI).

2.1.5 Power Requirements

The motors require 21 A to drive at maximum capacity when all of them are functioning simultaneously, and each motor operates at 24 V. The RPi required 1.5A at 5V, and the touchscreen and Arduino Uno together required 3 A at 12V to operate properly. The voltage provided by the batteries was 24 V, so voltage regulators were used in order to meet the 5 and 12 V requirements. Fuses in line with each motor controller, RPi and Arduino, were added to prevent any damage in the event of a short circuit.

2.2 Image Collection Procedure Using the Developed Phenotyping System

Since each image collected with the system covers only a portion of a mature energy sorghum plant, image stitching is required. This process can be done without distortion or misalignment for images collected with unmanned aerial vehicles (UAVs) when the images have an overlap between 75% and 45% (Jia et al., 2016). As the overlap area increases, the number of images required to cover a particular area increases, so in most cases an overlap greater than 75% is undesirable (Gómez-Candón et al., 2013). Therefore, the overlap area for the images collected in this work was set at 75%. The imaging system thus collected an image every 12 cm.

It was critical that the motors initiating the vertical movement of the imaging system have adequate torque, so a minimum f.s. of 2 was established. In order to achieve this f.s. at all speeds encountered, each motor had to output 2.8 N•m of torque at any speed. The speed-torque curve of the motors indicated that at 2.36 rps the motors would output approximately 2.8 N•m. The motors stepping at 400 steps per revolution and the fast-travel threaded rods allowed for 2.54 cm [1 in] per rotation. Therefore, the imaging system speed was set at 6 cm/s in the vertical direction.

The phenotyping platform system was tested at one of the greenhouses located in the Greenhouse Annex at Texas A&M University during the month of August 2016. The starting location of the camera system was set to the right-hand lower corner (assuming the handle is located on the right). The imaging system was programmed to move in only one direction at a time, either vertical or horizontal. There were two reasons for only moving in one direction. (1) Since most of the images collected are to

be stitched together in the vertical direction, the system was design to only move direction at a time. (2) This design limitation prevented miscalculation of imaging system location by the software, a problem that could be made more difficult by simultaneous vertical and horizontal motion. A schematic showing the possible travel path for the imaging system is shown in Figure 12.

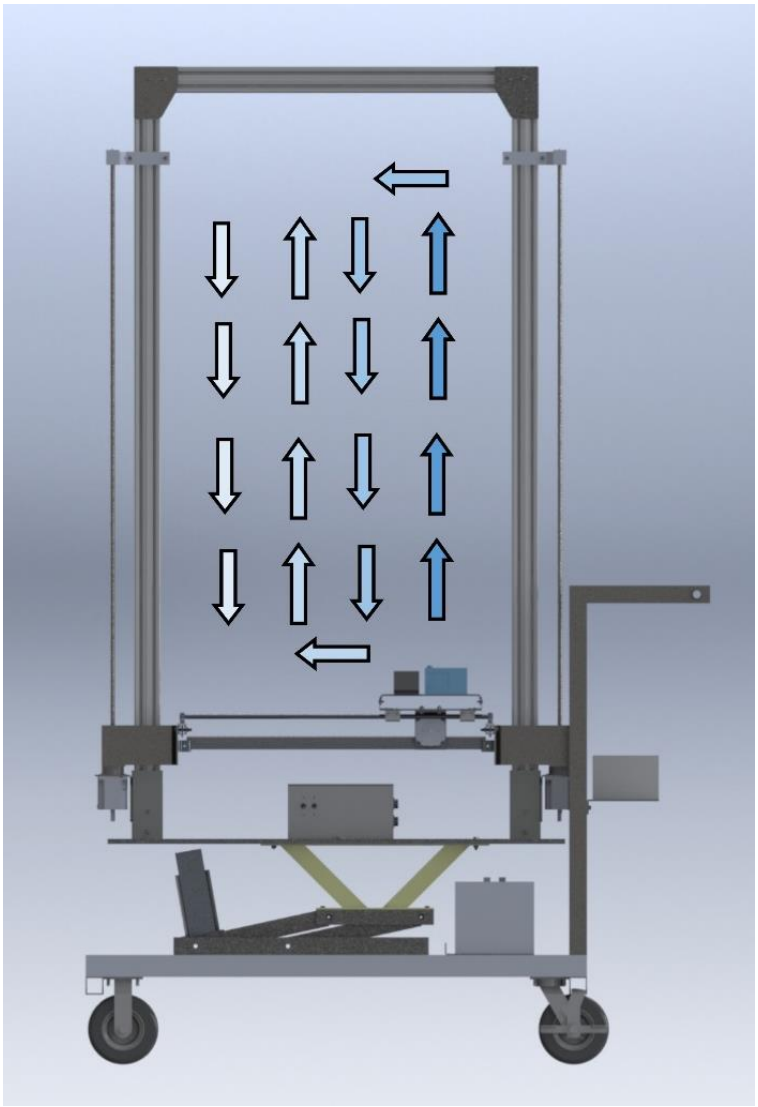

Figure 12. Possible path to be followed by the imaging system within the upper frame during the image collection process.

The phenotyping system was placed at the edge of the first plant in a row of sorghum plants. Images were collected from the first plant while the imaging system moved upward, then sliding over to the left and imaging the next plant as it moved downward. Then the same process was repeated. Up to 3 plants for every platform position could be imaged. Then the platform was moved to the next plant to continue the process.

The height range of the plants was between 1.0 and 3.5 meters tall. The taller plants were grown in the field, allowing them to grow taller than they would have in the greenhouse, and they were used to provide an estimate of how tall plants could be and still be imaged by the imaging system at its lowest setting; i.e., without using the lift mechanism. Images with the system at its highest setting could not be collected due to the height limitations of the particular greenhouse used for this test. However, the lift mechanism was expected to add 40 cm to the imaging height. The short plants were grown in the greenhouse with conditions similar to those in the field, with temperatures ranging between 24.2 ºC and 32.3 ºC. The energy sorghum variety used during this test was R.07020. These plants were provided by Dr. John Mullet, Professor of Biochemistry and Biophysics, Texas A&M University, who conducts research in energy sorghum. The genotype variety of energy sorghum was provided by Dr. Rooney, Professor of Soil and Crop Sciences, Texas A&M University, who specializes on sorghum breeding and genetics.

A total of 10 sets of images were collected with the phenotyping system, with between 10 and 15 images per set. Since these images were collecting during the

calibration and testing of the phenotyping system, the number of images in each set was dependent on plant size and the vertical distance the imaging system translated between images.

Sorghum stalks have cross-sectional shapes similar to an ellipse. The major axis is parallel to the direction in which leaves extend. Images were collected perpendicular to the major axis. The distance between the camera lens and the approximate halfway point of the plant stalk was measured to be approximately 50 cm. The CIR camera was used to collect images which were stored in the compact flash memory of the camera as .RAW files. These files were then converted to .TIF files with PixelWrench2 software (Tetracam, Inc., [Chatsworth, California, USA]). These processed images were used to evaluate image stitching software.

2.3 Image Collection Procedure to Measure Stalk-Thickness

A separate set of RGB images of energy sorghum varieties R.07019 and R.07007, both varieties provided by Dr. Mullet, were collected for the purpose of measuring stalk thickness. Four samples of each variety were grown in the greenhouse at temperatures generally between 24.2 ºC and 32.3 ºC and supplied with Osmocote 14-14-14 slow release fertilizer. One image of each plant was collected on a weekly basis for 10 weeks.

Images with 720 x 1280 pixels resolution were collected with an RGB camera (Creative Technology Ltd., [Milpitas, CA, USA]). In order to simplify image segmentation of plant matter from the background, a polyvinyl chloride (PVC) pipe

frame with dark cloth was used as a backdrop to isolate the plant from the greenhouse light environment at the time of image collection.

Again, images were collected perpendicular to the major axis. Manual measurements of the stalk diameter were collected with a caliper for later comparison to the measurements calculated with image analysis. The distance between the camera lens and the center of stalk of the sorghum plant being imaged was measured. This distance was used to determine the size of image pixels in the stalk diameter measurement algorithm.

2.4 Image Processing and Analysis

2.4.1 Image Stitching

One of the goals of this project was to demonstrate the ability of the phenotyping system to obtain phenotypic data from entire plants. The phenotyping platform is able to provide a set of images from a plant that can be stitched together to have a complete picture of the plant. This image-stitching process is part of image pre-processing. COTS software with image-stitching capability is readily available.

Two different criteria were used to assess image stitching software. (1) The accuracy and repeatability of the software in stitching images together; (2) the speed at which the images were stitched together on an i3 Intel Processor (Intel, [Santa Clara, California, CA]) computer with 8 GB of RAM. The images collected with the phenotyping system were used to assess Adobe Photoshop CS6 (Photoshop) and GIMP as potential stitching software. Accuracy was evaluated by observing whether the software would align the stalk and leaves of the plant accurately across images. If 8 of 10 images were well

aligned, the stitching attempt was considered acceptable. Repeatability was evaluated by loading different image sets and determining whether all of them were stitched together accurately. A stopwatch was used to determine total image stitching time. The results obtained were saved as .jpeg files without any compression. Four of the 10 image sets were selected for image stitching based on the quality of images in the set. Some images in certain image sets had lower brightness and did not show the plants as clearly. Others only imaged part of a plant and so were not appropriate for evaluating image stitching.

Photoshop has an option for automated stitching. Images are loaded into Photoshop, and the automated application runs feature matching and linear panorama algorithms to stitch the images together. Individual image sets were loaded to Photoshop at once. Then a stopwatch was started when the application started to stitch the images together. When the application completed the stitching process, the stopwatch was stopped. Results were visually assessed, with close attention paid to the alignment of the stalk and the leaves of the plants (Figure 13).

GIMP provides tools to precisely move, size, change transparency, and adjust color and brightness of images while performing manual stitching. GIMP enables loading all images at once. All the images were reduced from 1536 x 2048 pixels to 461 x 600 pixels, keeping the aspect ratio the same. In this way, images were handled easier by the user and software. The image of the lowest point in the stalk was placed at the bottom. Each image was then aligned to this image, making sure that the stalk and leaves in the images matched well. The same process was repeated for all images. No significant distortion from change of perspective or brightness was observed among the images. A

stopwatch was started when the images were loaded and stopped when all the images were stitched together. The results were then visually assessed, with close attention paid to possible locations where the images were not aligned well. The same image sets stitched together with Photoshop were also stitched together with GIMP.

Figure 13. Image showing example of criteria when assessing results of image stitching; the stalk and leaves alignment is shown.

2.4.2 Plant Segmentation Algorithm

Separating plant matter from the image background, or plant segmentation, is a crucial step that must be accomplished before performing any further image analysis. The K-means clustering algorithm, adapted from the work of Corke (Corke, 2011), was used in

this project to segment plant matter from the background. The algorithm performs color-based segmentation based on a pre-selected C number of clusters. Each RGB or CIR value is mapped to the color xy-chromaticity space and then segregated into image classes associated with those clusters. The algorithm initially selects locations in the data space as cluster centers and then calculates the Euclidean distance (Ghimire & Wang, 2012) between each pixel and every cluster center in multiple iterations. At the end of an iteration, each pixel is assigned to the cluster with the closest center, and every cluster center location is recalculated as the average location of the pixels assigned to that cluster. The final result is a classification of the image into C number of classes (Corke, 2011; Ghimire & Wang, 2012; Liang & Zhang, 2014; Sert & Okumus, 2014; Yu et al., 2014). The plant segmentation algorithm was applied to a unique set of whole-plant images collected in the laboratory, and each image was segmented, into ten classes. The user identified the five classes that best represented the plants based on whether or not the class clearly contained almost exclusively plant matter.

After segmentation, the noise in each class image was reduced by a morphological opening with a 9 x 9 square kernel. The five classes in the image were then combined into one, producing a binary image, and separating the plant matter from the background. The combined binary image was then processed by area opening to remove small artifacts. Finally, to reduce segmentation problems caused by plant lesions and minor stalk deformities, a morphological closing with a 5 x 5 square kernel was applied to the image. The result was a binary image of the plant segmented from the background.

Additionally, the plant segmentation algorithm was tested on stitched images to observe the algorithm's performance on CIR stitched images.

2.4.3 Stalk-Thickness Calculation Algorithm

Stalk thickness calculation involved an algorithm capable of automatically scanning the binary image and identifying the edges of the stalk. The calculation was performed in "supervised" and "unsupervised" modes. In the supervised mode, the user selected the location where the algorithm scanned for the stalk edges. The scanning kernel was a 3 x 3-window.

Once the edge pixels were identified by the algorithm, stalk thickness in pixels was calculated by subtracting the edge location on the right from the edge location on the left. In unsupervised mode, the user identified the stalk center and allowed the algorithm to select upper and lower stalk thickness measurement locations.

The average thickness based on the upper and lower measurements was taken as the stalk thickness. In both modes, stalk thickness in pixels was multiplied by the pixel-length conversion factor, which was dependent on the distance between plant and camera, to obtain stalk thickness in millimeters.

2.5 Statistical Analysis

The percent error between the stalk-thickness measurements obtained with image analysis and manual measurements was calculated. Outliers were observed in the data, affecting the comparison of the two measurement methods. In order to validate whether these data points were actually outliers, they were analyzed as follows: (1) Residuals

were calculated and plotted against the caliper measurements, and heteroscedasticity was indicated; (i.e., residual values were lower at low stalk thickness values and higher at high stalk thickness values). (2) Based on the fact that the residuals were heteroscedastic, both KMS and caliper measurements were transformed by taking their logarithms. Log(caliper) was regressed against log(KMS), and residuals were again plotted, indicating that heteroscedasticity had been mitigated. (3) Studentized residuals of the log(caliper) vs. log(KMS) relationship were calculated, and the distribution of the studentized residuals was determined. By observing the linear regression plot of the caliper and KMS, a total of seven data points were identified as possible outliers because of their distance to the distribution. In order to verify whether they were outliers, the studentized residual was identified for each data point. An outlier was considered as such if the studentized residual value was 2.5 or greater. The values of the seven identified data points were confirmed to be higher than 2.5.

(4) The original images associated with the suspected outliers were then inspected to determine whether anomalies that could produce major errors could be identified. With each of the suspected outliers, the images suggested that significant error-causing anomalies were present, so these data points were removed. After the removal of the outliers, the data were plotted in a linear regression graph.

3. RESULTS AND DISCUSSION*

3.1 Design, Construction and Testing of the Phenotyping System

The phenotyping platform system design is shown in Figure 14 along with the constructed system. Design features that are particularly notable in the constructed system include (1) the size of the phenotyping platform, which enabled the camera system to image up to 3-meter-tall energy sorghum plants and yet was suitable for use in greenhouses with 3.5-meter-high clearance. The narrow width (47 cm) allows for row spacing of 76 cm, a common row spacing in a greenhouse and sorghum field (Figure 14).

(2) The low center of gravity and mobility, which were achieved by building the lower frame of heavy material (A36 steel) and placing heavier components such as the batteries closer to the ground. The wheels attached to the chassis enabled good mobility in the greenhouse (one person alone could move the system to a desired location). The space on the chassis was adequate for the batteries, which were easy to access but also out of the way. The battery location also helped to reduce any shock hazard (Figure 15). The lift system was able to lift the upper frame without difficulty. The extension on the lift system's release and lift lever added safety during operation by allowing the user to stand next to the system instead of reaching underneath to lower it (Figure 15). Some vibration was observed on the upper section when the lift was operated. However, it did not affect the design structure.

*Part of this section is reprinted with permission from "Imaging for high-throughput phenotyping in energy sorghum" by Batz, J; Mendez-Dorado,M & Thomasson, J.A, 2016. Journal of Imaging, 2(4).

The upper frame is strong enough to withstand the design load, yet light enough so that the effect of the upper section on the center of gravity is minimal. In addition, corrosion is minimized in this section because of aluminum's material properties; eliminating corrosion is crucial to sections where there are moving parts that require precise control. The corner sections of the upper frame, built from steel, reinforced the joints and prevented misalignment.

Figure 14. Left: phenotyping system design rendering, fully assembled, including the controlling unit; right: phenotyping system prototype constructed, fully assembled.

Figure 15. Battery location within the built phenotyping system, kept away but easy access if needed.

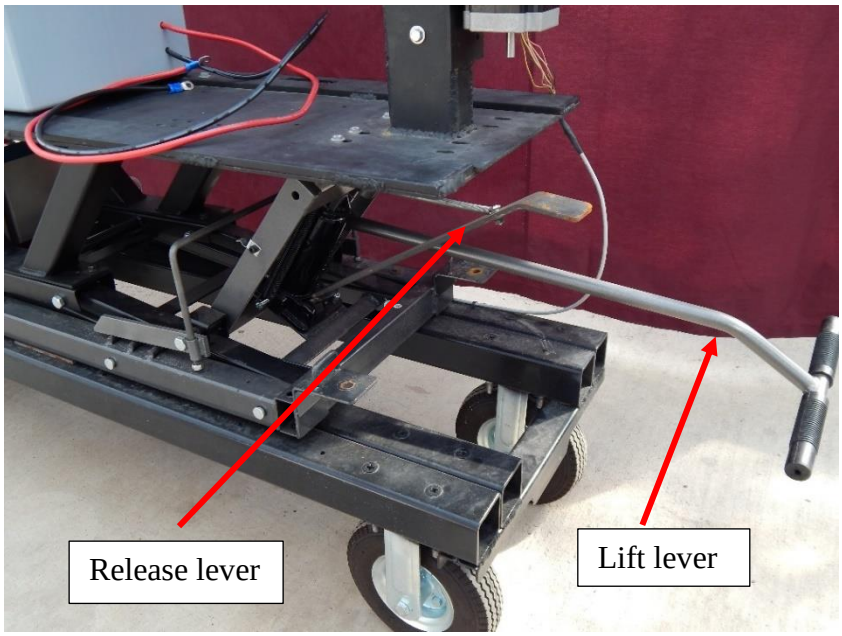

Figure 16. Lift lever and release lever, both extending out from underneath the phenotyping system to increase operational safety and convenience.

3.2 Phenotyping System Control and Imaging System Design

The embedded control unit of the phenotyping system, controlled principally by the RPi, worked as designed. The user-friendly GUI, controlled by the RPi, responded to human interaction without error. The Arduino, in slave mode to the RPi, executed the commands sent by the RPi effectively. The motor controllers responded accurately to the logical input from the Arduino, moving the two side motors in unison, and preventing misalignment as the camera system moved vertically.

The control box housing the motor controllers and power distribution unit also performed as designed, and it allowed for easy access and troubleshooting. The box that contained the touchscreen and micro-controllers also performed as designed. However, some glare was evident on the screen because of the amount of sunlight in the greenhouse. The glare observed on the touchscreen could be mitigated by using a touchscreen with a brighter screen setting than the one used in this project. The power supplied by the batteries was sufficient to operate all mechanisms under all conditions tested.

The user-friendly GUI offered an interactive method of controlling the phenotyping platform (Figure 17). The large font and buttons allowed for easy user input. The change in colors of the buttons when pressed helped the user to know the correct button was pressed. Each button had to be pressed individually, as the GUI did not respond to input while the imaging system moved except for the Stop button. In the manual mode, the imaging system moved vertically or horizontally depending on the direction selected (left, right, up, and down) in the GUI. A button labeled “center” returned the imaging

system to the starting location. In the auto mode, when the “2 ft [0.61 m]”, “4ft [1.21 m]”, “6ft [1.83 m]”, 8ft [2.44 m] button was pressed, the imaging system moved vertically 48,72, 96,120, and 144 cm, respectively. It paused every 12 cm to allow time for an image to be collected and then moved to the left and proceeded downward in the same sequence. When the “10 ft [3.05 m] button was pressed, the imaging system moved vertically 144 cm, in this case the additional height required to image 3.0 m was provided by the scissor lift. Since the test greenhouse had a lower height clearance, the scissor lift could only be extended 30 cm from the lowest position.

The imaging system demonstrated vertical mobility within the frame, as the threaded rods handled the weight of the camera system as designed, without slippage during testing of the system. The imaging system also moved side to side with ease as the rack and pinion system operated as designed. The motors consistently responded precisely to the distance directed by the control box, moving to the desired target position.

The time for the camera to take and store a single image was recorded and reported to be roughly 1 second. Since the shape of sorghum stalks is elliptical, it is crucial to specify the orientation in which images are collected and maintain camera alignment. If the orientation is not maintained, incorrect stalk thickness measurements will result. Plants were placed such that the CIR camera remained aligned to the wide stalk diameter throughout the testing process. A method to image stalk thickness in a way that is invariant to the orientation of the stalk could be potentially developed, but it was not within of the scope of this project. An example of a possible method could be the

implementation of a stereo vision system, utilizing information from two cameras to identify the orientation of the plant.

Figure 17. User-friendly Graphic User Interface (GUI), top: manual mode of operation; bottom: auto mode of operation, both used to control the camera articulation.

By translating the imaging system in 12 cm. increments, the area overlap achieved between images was approximately 75%. A total of 10 images were needed to image an entire sorghum plant with a height of 2.0 meters. At 12 cm., vertical increments and a speed of 6 cm/s, a total time of 85 seconds was needed to image a complete sorghum plant measuring 2.0 meters tall. For the design number of 288 plants per greenhouse, plants with a height of 2.0 meters would require 6.8 hours. The plants got taller by 5-10 cm during the testing stage of the phenotyping system so an entire plant taller than 2.2 meters could not be imaged. However, the following two assumptions could be made to estimate the total image collection time for the design 3-meter-tall plant. (1) Five images per meter of plants height, which for a design 3-meter-tall plant would require 15 images. (2) Dividing the total image collection time by the number of images required gives 8.5 seconds per image. Multiplying 8.5 seconds by 15 images gives an estimated time of 127 seconds to image a complete 3-meter-tall energy sorghum plant. Therefore, to image 288 entire energy sorghum plants 3-meter-tall, approximately 10.5 hours will be required. This time was only an estimate for image collection, it does not account for the time to move the cart and actuate the lift system.

There are two possible ways to reduce image collection time. (1) Reduce the overlap area of the images to 45%, as previous work suggested as being the lowest acceptable overlap (Jia et al., 2016). However, the reduced overlap may increase misalignment of the images or distortion. (2) Increase the speed at which the imaging system moves in the vertical direction. The f.s. of the motor performance could be reduced to a value closer to 1, however from an engineering stand point, this value is not recommended. As

f.s. value decreases and approaches 1, the motors operate closer to maximum capacity. At a f.s. of 1.5, 2.1 N•m of torque from each motor would be needed to move the imaging system vertically. Based on the speed-torque curve the motors could move at 3.5 rotations per second and consequently move the imaging system at approximately 8.80 cm/s. The increase in vertical speed would result in less time to collect images.

3.3 Image Stitching Tools Assessment

Examples of image-stitching results with Photoshop CS6 (Photoshop) and GIMP are shown in Figures 18 through 21. The overall results of image stitching showed that it was possible to stitch images together with 75% overlap.

However, Photoshop's automated stitching procedure did not give good results. In some image sets the stalk and leaves did not match across image seams, and stalks were not aligned (Figure 18). Out of the four image sets used for testing stitching software, Photoshop was only able to stitch two sets into a complete image. Photoshop did not use all the images loaded into the software. In one image set, for example, seven images were loaded to Photoshop, but only four were used by the software to perform image stitching. Figure 19 shows the result of this stitching test in which only four images were used to stitch an entire image together. It took Photoshop 10 to 15 min to stitch together 10 images. If for example, we consider loading 15 images from a 3.0-meter-tall plant, based on the number of images assumed needed, then Photoshop might take a longer than 15 minutes to process the images.

Figure 18. Result of image stitching with Photoshop, the image shows that parts of the plants is missing.

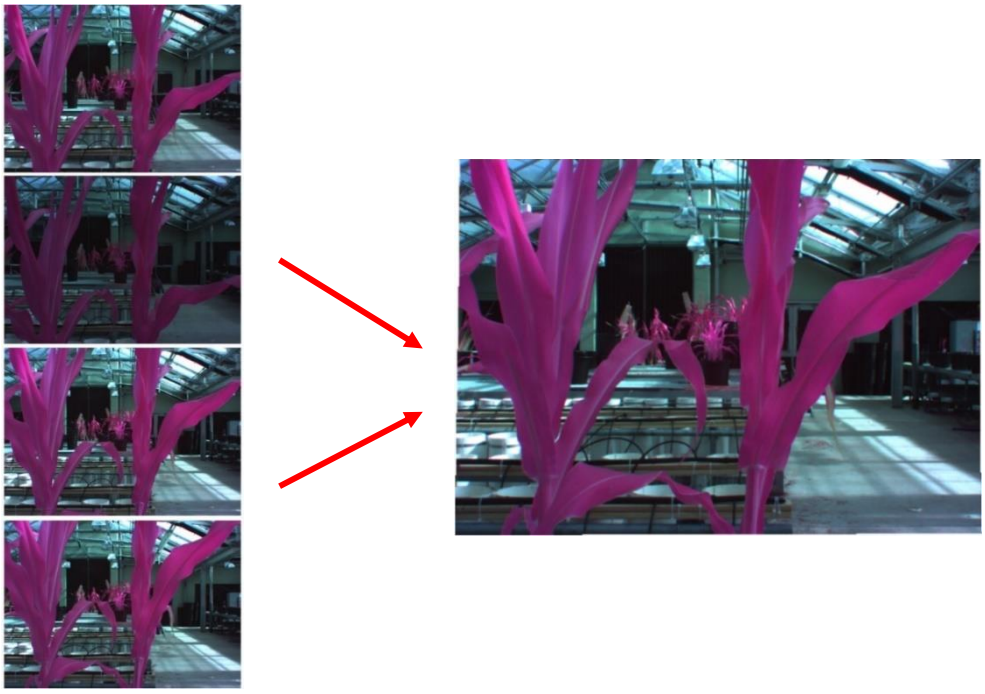

Figure 19. Image of energy sorghum plant stitched with Photoshop CS6, Photoshop only used 4 of 7 images to obtain this image; the plant size at this stage was roughly 95 cm tall.

Image stitching was much more effective with GIMP. An example set of 10 images, representing an entire plant, were stitched together to obtain Figure 20. The results of image stitching in GIMP had only minor misalignments on three images towards the top of the plant. The stitched images represented the entire energy sorghum plant. The total time to stitch these images together manually was about 8 minutes. Figure 21 is another example of image stitching performed with GIMP. This image set was collected during calibration of the phenotyping system. For this image, a set of 11 individual images were stitched together for a 1.5-meter tall plant.

By comparing the efficacy, repeatability and time between Photoshop and GIMP, it was clear that GIMP performed better at image stitching. However, manual image stitching took about 8 minutes per image set in GIMP, and it might take longer depending on user capability with the software. Photoshop might take 10-15 minutes per set but the time is more consistent because it is an automated process. Additionally, Photoshop was not able to stitch larger sets of complete plants, whereas GIMP was able to stitch image sets of complete plants correctly.

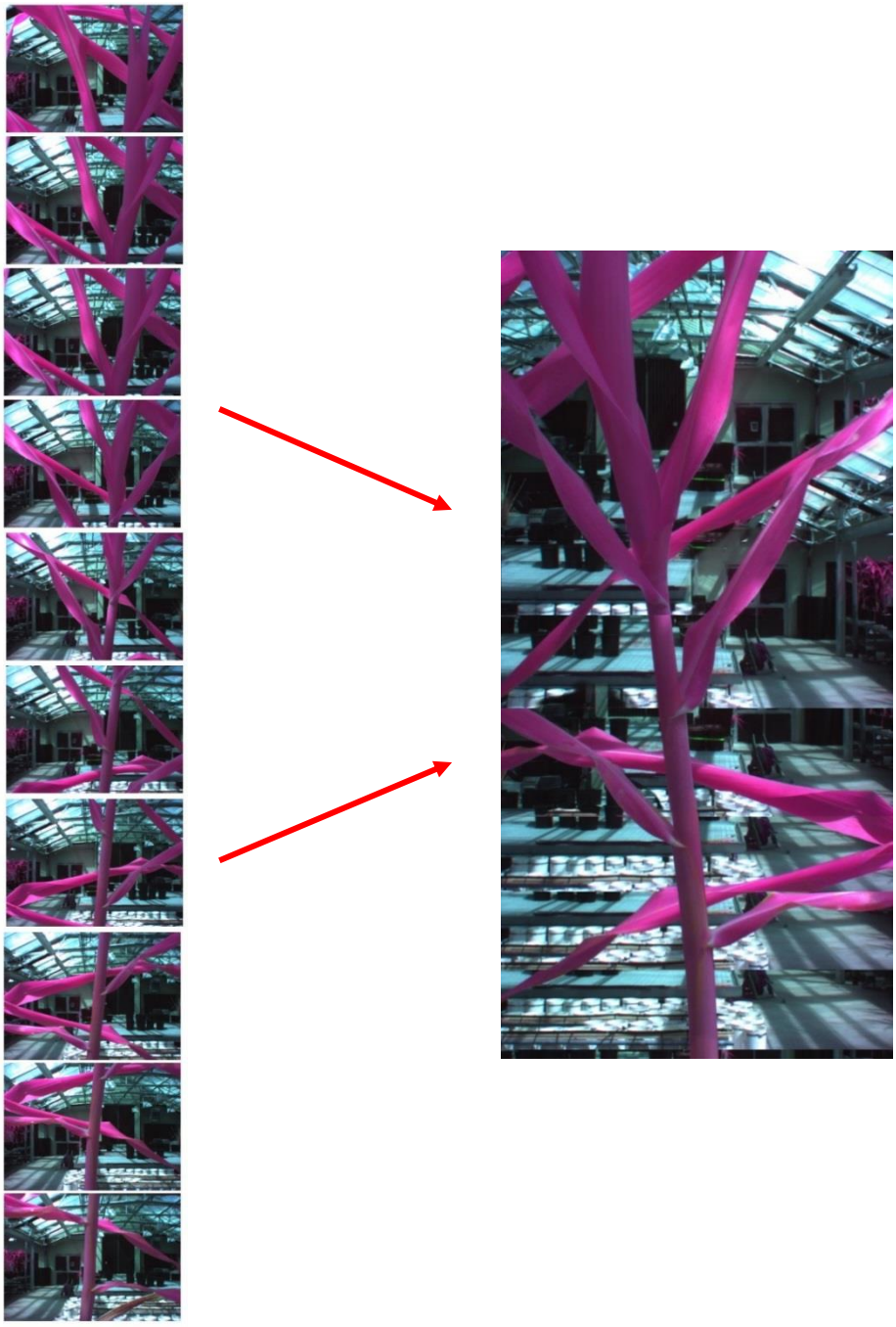

Figure 20. Result of image of sorghum plant stitched using GIMP, a total of 10 images were used to construct this image. The sorghum plant was roughly 180 cm tall at the time of imaging.

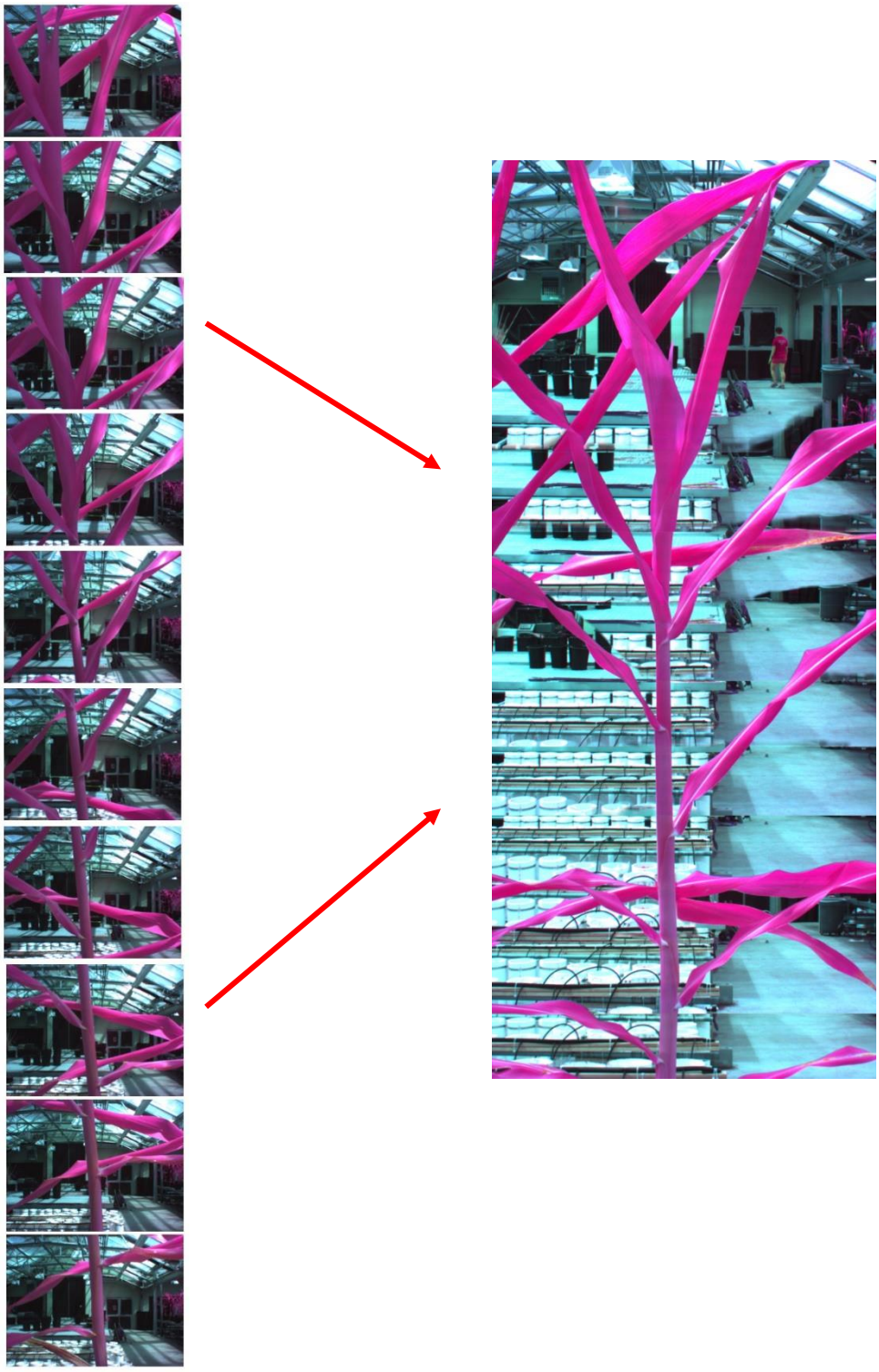

Figure 21. Result of image mosaic using 11 images collected with the phenotyping system. The plant imaged was roughly 150 cm tall.

3.4 Plant Segmentation and Stalk-Thickness Measurement Algorithms

Results of implementing the segmentation algorithm on the RGB and CIR images are shown in Figures 22 and 23, respectively. By considering the original CIR image and the segmented CIR image together, as an overlay (Figure 24), the results are made clearer. Figure 24 shows the CIR image only where the algorithm segmented it out as plant matter and the rest of the image as black. Some errors were observed in the results of the plant segmentation algorithm; some stalks and leaves were not segmented as plant matter and thus there are some missing parts of the plant, also some of the artifacts in the background got segmented as part of the plant (Figure 22). The better contrast between plant matter and other objects in the CIR images helped with image segmentation. An example of the application of the plant segmentation algorithm on CIR images is shown in Figure 23. Some horizontal lines were observed as artifacts in this particular example. This issue could be related to non-plant objects or to image stitching. A possible method to reduce the horizontal lines is to perform a morphological opening to the segmented image.

Figure 22. Image segmentation using K-means algorithm, applied to red, green and blue (RGB) images of energy sorghum plants.

Figure 23. Plant segmentation algorithm results using K-means algorithm on a color-infrared (CIR) image, left: original image; right: plant segmented from background.

Figure 24. Combination of the original image and segmented plant, the results show the efficacy of the plant segmentation algorithm used.

The results obtained from plant segmentation with RGB images (Figure 22) suggests that the algorithm was successful. Minor errors in the segmentation results (small parts of the plant missing) were observed, but not to the extent that the imaged plant could not be segmented reasonably well. The results obtained using CIR images suggest that the algorithm also works with this type of images. Again, the use of CIR images facilitates the process of plant segmentation. Overall results obtained from the plant segmentation algorithm showed that plant matter could be successfully segmented from the rest of the image. This step is critical in any image analysis algorithm.

When comparing the results of the stalk thickness measurement algorithm to manual caliper measurements, statistical analysis of the data showed that across all dates, the average percent errors were 27.9 for K-means with unsupervised stalk measurement (KMU), and 16.0 for K-means with supervised stalk measurement (KMS).

A linear regression comparing the stalk thickness values obtained with KMS-based image analysis to the values obtained with the caliper provided an R^2 value of 0.70, indicating that KMS measurements account for 70% of the variability in the caliper measurements (Figure 25).

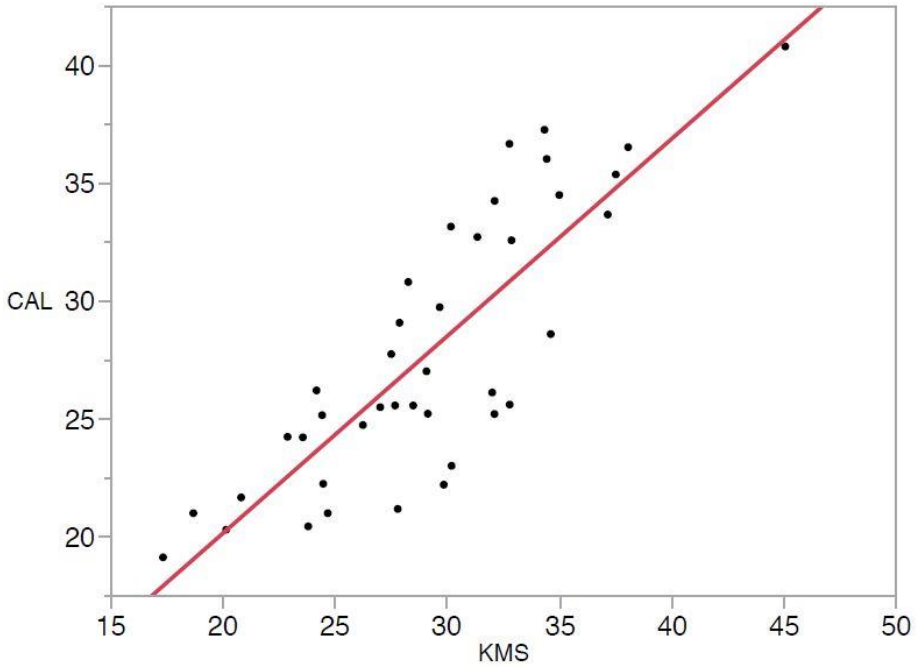

Figure 25. Linear regression, KMS values compared to the caliper values. The R^2 calculated for this relationship was 0.70.

By performing a time approximation, the phenotyping system would take 10.5 hours to image a design set of 288 plants measuring 3.0 meter-tall. The time to push the cart and lift the system would add 1-2 hours. This estimated time is based on the time it took to set up the system in the greenhouse during testing. In addition to the image collection time, the time to stitch images together and image analysis has to be considered. Given that it takes 5 to 8 min to process each image set, one set per plant. Then for 288 plants, a total time of to stitch images together with GIMP would be between 28 and 38 hours. Stalk-thickness measurements using image analysis would take between 3-4 hours for 288 plants. Image stitching is the most time-consuming task in the process as currently designed. Although this time is significant, more work could be devoted to identifying software capable of performing image stitching automatically in a timely manner. This would greatly reduce the time process images and take full advantage of throughput of the phenotyping system.

4 FUTURE WORK

Future work in the mechanical aspect of this project could be made to the platform structure so that it vibrates less when the lift system is actuated. Also, a lighter structure could be designed so that the phenotyping system is easier to handle in constrained spaces. In the programming aspect, more options and features could be added to the GUI. For example, a method could be added for the user to add meta-data to the images collected, explaining circumstances that are out of the ordinary. Another improvement would be to integrate a triggering system for the camera. The phenotyping system would then automatically take images. Using different cameras in the phenotyping system could also increase performance. For example, using a time-of-flight camera to measure the distance of the plant stalk to the camera would provide more accurate measurements than manual distance measurements. Improvements in image stitching are needed, either by developing a better image stitching algorithm or identifying software capable of performing automated image stitching with successful results. Stalk-thickness measurement also could be improved by automating the entire process, wherein the user would only have to upload the images and the algorithm would identify and measure the stalk without supervision. Eventually leading towards a phenotyping system capable of collecting, processing, and analyzing images automatically.

5 CONCLUSIONS

This project involved developing the required components of a system for phenotyping energy sorghum plants in a greenhouse. The phenotypic specific measurement of interest was stalk thickness, since it is a major factor in determining the biomass yield of the plant. The required components of the system are an automated sensor platform for the greenhouse, an image-stitching method to combine multiple images of individual plants taken at close range, and image-analysis methods to segment and measure stalk thickness. The phenotyping platform designed and constructed in this project proved capable of automatically collecting multiple color-infrared images representative of an entire energy sorghum plant from close range in a greenhouse. The estimated time to collect images of 288 complete energy sorghum plants was calculated to be between 14 and 15 hours. The phenotyping platform enabled the collection of images of energy sorghum plants up to 3.0 meters tall. The phenotyping platform in this project showed the possibility of imaging large numbers of energy sorghum plants in a greenhouse at close proximity. The advantages of this system include flexibility of use in different greenhouses and low maintenance. Furthermore, the research determined that GIMP software was capable of being used for manual stitching of the images into a large mosaicked image of an individual plant with acceptable accuracy. Results obtained with GIMP acted as a bridge between the phenotyping system and image analysis to obtain phenotypic data of stalk thickness. The image analysis techniques and algorithms developed in this project, specifically for plant segmentation and stalk measurement, gave promising results in measuring the stalk thickness of energy sorghum plants, with

an average 16 % error relative to manual measurements. Obtaining useful phenotypic measurements of energy sorghum with image analysis, in a mostly automated fashion, is now feasible based on the results on the results of this work. This research has paved a portion of the path towards an increased rate of bioenergy crop improvement.

REFERENCES

Andrade-Sanchez, P., Heun, J. T. (. 1.)., Gore, M.A. (2,3), Thorp, K. R. (. 2.)., Carmo-Silva, A., French, A. N. (. 2.)., White, J. W. (. 2.). (2014). Development and evaluation of a field-based high-throughput phenotyping platform. *Functional Plant Biology, 41*(1), 68-79. doi:10.1071/FP13126

Batz, J., Mendez-Dorado, M. A., & Thomasson, J. A. (2016). Imaging for high-throughput phenotyping in energy sorghum. *Journal of Imaging, 2*(4), 1-12.

Busemeyer, L. (. 1.)., Mentrup, D. (. 1.)., Möller, K. (1), Wunder, E. (. 1.)., Ruckelshausen, A. (. 1.)., Alheit, K. (. 2.)., . . . Rahe, F. (. 4.). (2013). Breedvision - A multi-sensor platform for non-destructive field-based phenotyping in plant breeding. *Sensors (Switzerland), 13*(3), 2830-2847. doi:10.3390/s130302830

Corke, P. I. (2011). *Robotics, vision and control: Fundamental algorithms in MATLAB® peter corke* Berlin: Springer, 2011]. Retrieved from http://lib-ezproxy.tamu.edu:2048/login?url=http://search.ebscohost.com/login.aspx?direct=true&db=cat03318a&AN=tamug.3932761&site=eds-live; http://lib-ezproxy.tamu.edu:2048/login?url=http://dx.doi.org/10.1007/978-3-642-20144-8

Diago, M., Correa, C., Millán, B., Barreiro, P., Valero, C., & Tardaguila, J. (2012). Grapevine yield and leaf area estimation using supervised classification methodology on RGB images taken under field conditions. *Sensors (14248220), 12*(12), 16988-17006. doi:10.3390/s121216988

Duda, M. M., Barascu, N., & Olteanu, G. (2016). Study of dynamics SPAD and NDVI values of potato plants according to the differentiated fertilization. *Bulletin of the University of Agricultural Sciences & Veterinary Medicine Cluj-Napoca.Agriculture, 73*(1), 5-14. doi:10.15835/buasvmcn-agr:12003

Dworak, V., Selbeck, J., Dammer, K. H., Hoffmann, M., Zarezadeh, A. A., & Bobda, C. (2013). *Strategy for the development of a smart NDVI camera system for outdoor plant detection and agricultural embedded systems* Retrieved from http://lib-ezproxy.tamu.edu:2048/login?url=http://search.ebscohost.com/login.aspx?direct=true&db=edswsc&AN=000315403300009&site=eds-live

Fraas, S., & Lüthen, H. (2015). Novel imaging-based phenotyping strategies for dissecting crosstalk in plant development. *Journal of Experimental Botany, 66*(16), 4947-4955. doi:10.1093/jxb/erv265

Gao, M., Van der Heijden, G. W. A. M., Vos, J., Eveleens, B. A., & Marcelis, L. F. M. (2012). Estimation of leaf area for large scale phenotyping and modeling of rose genotypes. *Scientia Horticulturae, 138*, 227-234. doi:http://dx.doi.org/10.1016/j.scienta.2012.02.014

Gheorghe, G. (2015). Climate changes - causes, effect and provisions to diminish the impact. *Annals of 'Constantin Brancusi' University of Targu-Jiu.Engineering Series*, (4), 224-229. Retrieved from http://lib-

ezproxy.tamu.edu:2048/login?url=http://search.ebscohost.com/login.aspx?direct=true&db=e5h&AN=112256779&site=eds-live

Ghimire, S., & Wang, H. (2012). Classification of image pixels based on minimum distance and hypothesis testing. *Computational Statistics and Data Analysis, 56,* 2273-2287. doi:10.1016/j.csda.2012.01.005

Golzarian, M. R., Frick, R. A., Rajendran, K., Berger, B., Roy, S., Tester, M., & Lun, D. S. (2011). Accurate inference of shoot biomass from high-throughput images of cereal plants. *Plant Methods, 7*(1), 1-11. doi:10.1186/1746-4811-7-2

Gómez-Candón, D., Castro, A., & López-Granados, F. (2014). Assessing the accuracy of mosaics from unmanned aerial vehicle (UAV) imagery for precision agriculture purposes in wheat. *Precision Agriculture, 15*(1), 44-56. doi:10.1007/s11119-013-9335-4

Granier, C., Aguirrezabal, L., Chenu, K., Cookson, S. J., Dauzat, M., Hamard, P., . . . Tardieu, F. (2006). *PHENOPSIS, an automated platform for reproducible phenotyping of plant responses to soil water deficit in arabidopsis thaliana permitted the identification of an accession with low sensitivity to soil water deficit* Blackwell Science. Retrieved from http://lib-ezproxy.tamu.edu:2048/login?url=http://search.ebscohost.com/login.aspx?direct=true&db=edsjsr&AN=edsjsr.3694701&site=eds-live

Green, J. M., Appel, H., Rehrig, E. M., Harnsomburana, J., Chang, J., Balint-Kurti, P., & Shyu, C. (2012). PhenoPhyte: A flexible affordable method to quantify 2D phenotypes from imagery. *Plant Methods,* (1) Retrieved from http://lib-ezproxy.tamu.edu:2048/login?url=http://search.ebscohost.com/login.aspx?direct=true&db=edsagr&AN=edsagr.US201400089463&site=eds-live

Großkinsky, D. K., Svensgaard, J., Christensen, S., & Roitsch, T. (2015). Plant phenomics and the need for physiological phenotyping across scales to narrow the genotype-to-phenotype knowledge gap. *Journal of Experimental Botany, 66*(18), 5429-5440. doi:10.1093/jxb/erv345

Hao, B. (. 1.)., Xue, Q. (. 1.)., Bean, B. W. (. 2.)., Becker, J. D. (. 2.)., & Rooney, W. L. (. 3.). (2014). Biomass production, water and nitrogen use efficiency in photoperiod-sensitive sorghum in the texas high plains. *Biomass and Bioenergy, 62*, 108-116. doi:10.1016/j.biombioe.2014.01.008

Hartmann, A., Czauderna, T., Hoffmann, R., Stein, N., & Schreiber, F. (2011). HTPheno: An image analysis pipeline for high-throughput plant phenotyping. *BMC Bioinformatics, 12*, 148-148. doi:10.1186/1471-2105-12-148

Hund, A., Trachsel, S., & Stamp, P. (2009). Growth of axile and lateral roots of maize: I development of a phenotying platform. *Plant & Soil, 325*(1), 335-349. doi:10.1007/s11104-009-9984-2

OECD/IEA ©. (2015). *Key world energy statistics. IEA Publishing.* Licence: www.iea.org/t&c.

Jensen, T., Apan, A., Young, F., & Zeller, L. (2007). Detecting the attributes of a wheat crop using digital imagery acquired from a low-altitude platform. *Computers and Electronics in Agriculture,* Retrieved from http://lib-ezproxy.tamu.edu:2048/login?url=http://search.ebscohost.com/login.aspx?direct=true&db=edsagr&AN=edsagr.US201300831655&site=eds-live

Jia, Y. (2016). UAV remote sensing image mosaic and its application in agriculture. *International Journal of Smart Home, 10*(5), 159-170. doi:10.14257/ijsh.2016.10.5.15

Kipp, S., Mistele, B., Baresel, P., & Schmidhalter, U. (2014). High-throughput phenotyping early plant vigour of winter wheat. *European Journal of Agronomy, 52*, 271-278. doi:10.1016/j.eja.2013.08.009

Klukas, C., Chen, D., & Pape, J. (2014). Integrated analysis platform: An open-source information system for high-throughput plant phenotyping. *Plant Physiology, 165*(2), 506-518. doi:10.1104/pp.113.233932

Koçar, G., & Civaş, N. (2013). An overview of biofuels from energy crops: Current status and future prospects. *Renewable and Sustainable Energy Reviews, 28*, 900-916. doi:10.1016/j.rser.2013.08.022

Lamb, D. W., Schneider, D. A., & Stanley, J. N. (2014). Combination active optical and passive thermal infrared sensor for low-level airborne crop sensing. *Precision Agriculture, 15*(5), 523-531. doi:10.1007/s11119-014-9350-0

Liang, B., & Zhang, J. (2014). KmsGC: An unsupervised color image segmentation algorithm based on K-means clustering and graph cut. *Mathematical Problems in Engineering*, 1-13. doi:10.1155/2014/464875

Lofton, J., Tubana, B. S., Kanke, Y., Teboh, J., Viator, H., & Dalen, M. (2012). Estimating sugarcane yield potential using an in-season determination of normalized difference vegetative index. *Sensors (14248220), 12*(6), 7529-7547. doi:10.3390/s120607529

Mulla, D. J. (2013). Twenty five years of remote sensing in precision agriculture: Key advances and remaining knowledge gaps. *Biosystems Engineering,* (4) Retrieved from http://lib-ezproxy.tamu.edu:2048/login?url=http://search.ebscohost.com/login.aspx?direct=true&db=edsagr&AN=edsagr.US201500163460&site=eds-live

Mullet, J., Morishige, D., McCormick, R., Truong, S., Hilley, J., McKinley, B., . . . Rooney, W. (2014). Energy Sorghum—a genetic model for the design of C4 grass bioenergy crops. *Journal of Experimental Botany,* (13) Retrieved from http://lib-ezproxy.tamu.edu:2048/login?url=http://search.ebscohost.com/login.aspx?direct=true&db=edsagr&AN=edsagr.US201500074393&site=eds-live

Neiff, N., Dhliwayo, T., Suarez, E. A., Burgueno, J., & Trachsel, S. (2015). Using an airborne platform to measure canopy temperature and NDVI under heat stress in maize. *Journal of Crop Improvement, 29*(6), 669-690. doi:10.1080/15427528.2015.1073643

Olson, S. (2012). High biomass yield energy sorghum: Developing a genetic model for C4 grass bioenergy crops. *Biofuels, Bioproducts & Biorefining, 6*(6), 640-655. doi:10.1002/bbb.1357

Olugbara, O. O., Adetiba, E., & Oyewole, S. A. (2015). Pixel intensity clustering algorithm for multilevel image segmentation. *Mathematical Problems in Engineering, 2015,* 1-19. doi:10.1155/2015/649802

Pajares, G., Peruzzi, A., & Gonzalez-de-Santos, P. (2013). Sensors in agriculture and forestry. *Sensors (14248220), 13*(9), 12132-12139. doi:10.3390/s130912132

Passioura, J. B. (2012). Phenotyping for drought tolerance in grain crops: When is it useful to breeders? [electronic resource]. *Functional Plant Biology, 39*(11), 851-859. doi:http://dx.doi.org/10.1071/FP12079

Reuss, A. (2015). Climate change: What is it? what causes it? what can we do about it? *Dollars & Sense,* (317), 34. Retrieved from http://lib-ezproxy.tamu.edu:2048/login?url=http://search.ebscohost.com/login.aspx?direct=true&db=f6h&AN=102142273&site=eds-live

Romano, G., Zia, S., Spreer, W., Sanchez, C., Cairns, J., Araus, J. L., & Müller, J. (2011). Use of thermography for high throughput phenotyping of tropical maize adaptation in water stress. *Computers and Electronics in Agriculture,* (1) Retrieved from http://lib-ezproxy.tamu.edu:2048/login?url=http://search.ebscohost.com/login.aspx?direct=true&db=edsagr&AN=edsagr.US201400024004&site=eds-live

Rooney, W. L., Blumenthal, J., Bean, B., & Mullet, J. E. (2007). *Designing sorghum as a dedicated bioenergy feedstock* Retrieved from http://lib-ezproxy.tamu.edu:2048/login?url=http://search.ebscohost.com/login.aspx?direct=true&db=edswsc&AN=000261819000016&site=eds-live

Sert, E. & Okumus, I. T., (2014). *Segmentation of mushroom and cap width measurement using modified K-means clustering algorithm* Retrieved from http://lib-ezproxy.tamu.edu:2048/login?url=http://search.ebscohost.com/login.aspx?direct=true&db=aci&AN=100016577&site=eds-live

Singh, A., Ganapathysubramanian, B., Singh, A. K., & Sarkar, S. (2016). Feature review: Machine learning for high-throughput stress phenotyping in plants. *Trends in Plant Science, 21*, 110-124. doi:10.1016/j.tplants.2015.10.015

Tazoe, Y., Sazuka, T., Yamaguchi, M., Saito, C., Ikeuchi, M., Kanno, K., . . . Makino, A. (2016). Growth properties and biomass production in the hybrid C4 crop sorghum bicolor. *Plant & Cell Physiology, 57*(5), 944-952. doi:10.1093/pcp/pcv158

Tuberosa, R. (2012). Phenotyping for drought tolerance of crops in the genomics era. *Frontiers in Physiology, 3*, 1-26. doi:10.3389/fphys.2012.00347

Van Der Heijden, G., Song, Y., Horgan, G., Polder, G., Dieleman, A., Glasbey, C. (2012). SPICY: Towards automated phenotyping of large pepper plants in the greenhouse. *Functional Plant Biology, 39*(11), 870-877. doi:10.1071/FP12019

Walter, A., Studer, B., & Kölliker, R. (2012). Advanced phenotyping offers opportunities for improved breeding of forage and turf species. *Annals of Botany*, (6) Retrieved from http://lib-ezproxy.tamu.edu:2048/login?url=http://search.ebscohost.com/login.aspx?direct=true&db=edsagr&AN=edsagr.US201500057314&site=eds-live

Watts, R. G. (2013). *Engineering response to climate change. 2nd ed. edited by robert G. watts* Boca Raton : CRC Press, Taylor & Francis, 2013]; 2nd ed. Retrieved from http://lib-ezproxy.tamu.edu:2048/login?url=http://search.ebscohost.com/login.aspx?direct=true&db=cat03318a&AN=tamug.4519207&site=eds-live; http://lib-ezproxy.tamu.edu:2048/login?url=http://www.crcnetbase.com/isbn/978-1-4398-8847-6

White, J. W., Andrade-Sanchez, P., Gore, M. A., Bronson, K. F., Coffelt, T. A., Conley, M. M., . . . Wang, G. (2012). Field-based phenomics for plant genetics research. *Field Crops Research, 133*, 101-112. doi:10.1016/j.fcr.2012.04.003

Yu, W., Wang, J., & Ye, L. (2014). An improved normalized cut image segmentation algorithm with k-means cluster. *Applied Mechanics & Materials*, (548-549), 1179-1184. doi:10.4028/www.scientific.net/AMM.548-549.1179